Published in final edited form as:
Dev Biol. 2013 February 1; 374(1): 96–107. doi:10.1016/j.ydbio.2012.11.020.

Deciphering Gene Expression Program of MAP3K1 in Mouse Eyelid Morphogenesis

Chang Jin[1,2], **Jing Chen**[1], **Qinghang Meng**[1], **Vinicius Carreira**[1], **Neville N. C. Tam**[1], **Esmond Geh**[1], **Saikumar Karyala**[1], **Shuk-Mei Ho**[1], **Xiangtian Zhou**[2], **Mario Medvedovic**[1], and **Ying Xia**[1]

[1]Department of Environmental Health, University of Cincinnati, College of Medicine

[2]School of Optometry and Ophthalmology and Eye Hospital, Wenzhou Medical College, Wenzhou, China

Abstract

Embryonic eyelid closure involves forward movement and ultimate fusion of the upper and lower eyelids, an essential step of mammalian ocular surface development. Although its underlying mechanism of action is not fully understood, a functional mitogen-activated protein kinase kinase kinase 1 (MAP3K1) is required for eyelid closure. Here we investigate the molecular signatures of MAP3K1 in eyelid morphogenesis. At mouse gestational day E15.5, the developmental stage immediately prior to eyelid closure, MAP3K1 expression is predominant in the eyelid leading edge (LE) and the inner eyelid (IE) epithelium. We used Laser Capture Microdissection (LCM) to obtain highly enriched LE and IE cells from wild type and MAP3K1-deficient fetuses and analyzed genome-wide expression profiles. The gene expression data led to the identification of three distinct developmental features of MAP3K1. First, MAP3K1 modulated Wnt and Sonic hedgehog signals, actin reorganization, and proliferation only in LE but not in IE epithelium, illustrating the temporal-spatial specificity of MAP3K1 in embryogenesis. Second, MAP3K1 potentiated AP-2α expression and SRF and AP-1 activity, but its target genes were enriched for binding motifs of AP-2α and SRF, and not AP-1, suggesting the existence of novel MAP3K1-AP-2α/SRF modules in gene regulation. Third, MAP3K1 displayed variable effects on expression of lineage specific genes in the LE and IE epithelium, revealing potential roles of MAP3K1 in differentiation and lineage specification. Using LCM and expression array, our studies have uncovered novel molecular signatures of MAP3K1 in embryonic eyelid closure.

Keywords

Laser Capture Microdissection; Expression Array; Embryonic Eyelid Closure; signaling pathways

INTRODUCTION

MAP3K1, also known as MEK kinase 1 (MEKK1), is a serine/threonine protein kinase of the MAP3K superfamily (Davis, 1995). This family consists of at least 21 members,

Correspondence should be addressed to: Ying Xia, PhD, University of Cincinnati College of Medicine, Department of Environmental Health, 3223 Eden Avenue, Kettering Laboratory, Suite 410, PO Box 670056, Cincinnati, OH 45267-0056, Phone: 513-558-0371, ying.xia@uc.edu.

responsible for activation of the MAP2K-MAPK cascades and regulation of a wide variety of biological functions (Craig et al., 2008). *In vitro* studies show that MAP3K1 specifically activates the MAP2K4 and MAP2K7 kinases, which in turn phosphorylate the c-Jun N-terminal kinases (JNKs) and/or p38 MAPKs, whereas *in vivo* studies have shown that MAP3K1 has diverse roles in the biological systems (Xia et al., 1998;Yan et al., 1994;Yujiri et al., 1998). The *in vivo* data collectively show that MAP3K1 regulates T and B cell-mediated immune responses, erythropoiesis and cardiogenesis; in addition, MAP3K1 plays a pivotal role in ocular surface morphogenesis during embryonic development (Gallagher et al., 2007;Gao et al., 2004;Geh et al., 2011;Labuda et al., 2006;Minamino et al., 2002;Venuprasad et al., 2006).

Mammalian ocular surface development involves the transient closure and re-opening of the eyelid (Findlater et al., 1993). In mice, eyelid development begins at embryonic day 12–13 (E12-13), when the surface ectoderm adjacent to the developing cornea folds to form the lid buds. The eyelid at this stage is a simple structure consisting of surface periderm covering undifferentiated mesenchyme. From E13 onward, the eyelid grows toward the center of the ocular surface. Between E15.5 and E16, a massive morphological change occurs at the junction of the outer and inner eyelid epithelium, causing the eyelid tip cells to elongate and migrate, leading to ultimate fusion of the upper and lower eyelids. Mouse eyelid remains closed between E16.5 and postnatal day 12–14, during which time the outer layer epithelium differentiates towards epidermis, the inner layer becomes conjunctiva, and the underlying mesenchyme derived from the migrating neural crest cells begins to form muscle, tarsus and other connective tissues. Eyelid re-opening takes place two weeks after birth, when cells at the fusion junction undergo apoptosis separating the upper and lower eyelids. While mice with normal embryonic eyelid closure have their eyelids closed at birth, mice with defective embryonic eyelid closure exhibit an eye open-at-birth (EOB) phenotype.

In mice, deletion of either the full-length (MAP3K1-null or $Map3k1^{-/-}$) or the kinase domain ($Map3k1^{\Delta KD/\Delta KD}$) of MAP3K1 results in the EOB phenotype (Yujiri et al., 2000;Zhang et al., 2003). Immunohistochemical analyses show that the $Map3k1^{\Delta KD/\Delta KD}$ fetuses have decreased phosphorylation of MAP2K4 and JNK in the eyelid tip epithelial cells (Takatori et al., 2008), whereas genetic studies show that although one functional *Map3k1* allele is sufficient for normal eyelid closure, it becomes haploinsufficient for eyelid closure in $Jnk1^{-/-}$ and $Jnk1^{+/-}Jnk2^{+/-}$ mice. These observations suggest that MAP3K1 regulates at least partly embryonic eyelid closure through activation of the MAP2K4-JNK pathways.

c-Jun, a member of the AP-1 group of transcription factors, is a potential downstream effector of this pathway. Phosphorylation of c-Jun by JNK at the N-terminal serine 63 and 73 is an important mechanism of AP-1 activation, because N-terminal phosphorylation promotes c-Jun dissociation from a transcriptional repressor complex, resulting in transcriptional activation of target genes (Aguilera et al., 2011). We showed that c-Jun N-terminal phosphorylation and AP-1 activity was much lower in the eyelid tip epithelial cells of $Map3k1^{\Delta KD/\Delta KD}$ compared to wild type fetuses (Geh et al., 2011;Takatori et al., 2008). However, lacking c-Jun phosphorylation cannot be responsible solely for defective eyelid closure. Transgenic mice harboring a mutant c-Jun with serines 63 and 73 replaced by alanines {c-Jun (AA)} completely lack c-Jun N-terminal phosphorylation, but have normal eyelid development (Behrens et al., 1999), suggesting that phosphorylation of c-Jun is dispensable for embryonic eyelid closure. Hence, the MAP3K1-JNK axis must regulate eyelid closure through other downstream effectors whose identities are still unknown.

In the present work, we have used global gene expression analyses to identify regulatory processes downstream of MAP3K1 critical in eyelid development. We found that MAP3K1

was abundantly expressed in the eyelid leading edge (LE) and inner eyelid (IE) epithelium of the developing fetuses. We used Laser Capture Microdissection (LCM) to isolate these cells from wild type and *Map3k1*$^{\Delta KD/\Delta KD}$ fetuses at embryonic day 15.5, a developmental stage immediately prior to eyelid closure. Gene expression signatures in LE and IE cells provide novel insights into the role that MAP3K1 plays in eyelid morphogenesis.

MATERIALS AND METHODS

Experimental animals, cells and reagents

Map3k1$^{+/\Delta KD}$ mice were previously described (Xia et al., 2000;Zhang et al., 2003) and were backcrossed to the C57BL/6 background for 7 generations. The fetuses were collected at E15.5 and genotypes were determined by PCR. Experiments conducted with these animals have been approved by the University of Cincinnati Animal Care and Use Committee. Antibody for β-catenin was from Sigma, phospho-H3 was from Millipore, α2-actin and SK myosin were from Thermal Scientific and Abcam, respectively. The HEK293 cells were purchased from American Type Culture Collection (ATCC). The Wnt3a expression vector, TCF/LEF DNA-binding sites-driven luciferase reporter (TCF/LEF-luc) and SRE-luc plasmids were kindly provided by Drs. Xinhua Lin (Cincinnati Children's Hospital Medical Center), Yujin Zhang (University of Cincinnati), and Jinsong Zhang (University of Cincinnati), respectively (Belenkaya et al., 2008;Hu et al., 2011). The AP-1-luc, SBE-luc and the MAP3K1 mammalian expression vector were described before (Zhang et al., 2005). The wild type {MAP3K1(WT)} and kinase-inactive {MAP3K1(KM)} mammalian expression plasmids were described before (Xia et al., 1998).

Tissue and cell preparation, RNA and cDNA generation and microarray

For LCM, the heads of E15.5 fetuses were embedded in Tissue-Tek OCT medium (Sakura Finetek USA) and stored in −80 °C. Eight μm coronal sections were mounted on plain uncoated glass slides, dehydrated and stained with HistoGene LCM frozen section staining kit, and were used for LCM following the manufacturer's protocol (Molecular Devices). Cells from 4 sections were collected on one LCM cap within one hour of collection to avoid RNA degradation. The cells were lysed in 100 μl Trizol (Invitrogen, Carlsbad, CA) at room temperature for 5 min and stored at −80 °C. It was estimated that 50 sections (12 caps) were processed for each fetus, which together generated 2,000 cells from the LE and 3,000 cells from the IE eyelid epithelium. The lysates from each fetus were pooled and processed as one biological sample.

The lysates were mixed with 0.1% Linear Acrylamide (Ambion, Austin, TX) and RNA was extracted by 2 rounds of chloroform phase separation and isopropanol precipitation, followed by washing three times with 75% ethanol. Samples were air dried and dissolved in 10 μl nuclease-free water. It was estimated that 10 ng and 15 ng total RNA were obtained from LE and IE eyelid epithelium, respectively, per fetus. RNA was analyzed by Agilent 2100 Bioanalyzer (Agilent, Santa Clara, CA) and samples with RNA Integrity Number (RIN) > 5.5 were processed for cDNA amplification. cDNA amplification and biotinylation was done using Ovation Pico WTA System (NuGEN, San Carlos, CA) following the manufacturer's instructions. Specifically, RNA (10 ng) was processed into first strand cDNA, a DNA/RNA heteroduplex, and thereafter a linear isothermal amplified cDNA. The amplified cDNA was purified with a PCR Purification Kit (QIAGEN, Valencia, CA).

The cDNAs from each fetus were considered one biological sample and 3 samples of each genotype were used for triplicate hybridization on the Affymetrix GeneChip Mouse Gene 1.0 ST array (P/N 901168, Affymetrix, Santa Clara, CA). The arrays are hybridized with 15 ug of fragmented aRNA. The hybridization, staining, and washing are carried out using the

Affymetrix GeneChip Hybridization Wash and Stain Kit (P/N 900720) following the manufacturer's protocols. The arrays are hybridized for 16 hr at 45°C using Affymetrix Hybridization Oven 640 (P/N 800139). FS450_0001 protocol is used for staining and washing the GeneChips using the Affymetrix Fluidics Station 450 (P/N 00-0079). The GeneChips are scanned with Affymetrix GeneChip Scanner 3000 7G Plus using Affymetrix GeneChip Command Console 3.2.3.1515 software and Affymetrix preset settings.

Quantitative RT-PCR

Quantitative PCR was performed using an MX3000p thermal cycler system and SYBR Green QPCR Master Mix (Stratagene), using conditions optimized for each target gene primers with efficiency greater than 85%, cycles less than 28 and sample locations on the plates been randomized. The PCR products were subjected to melting curve analysis and the relative cycle differences in qRT-PCR were determined using ΔCt, as described (Schnekenburger et al., 2007). The ΔCt value for each sample was determined using the cycle threshold (Ct) value of the specific gene normalized to that of *Gapdh*. The fold change was calculated based on the ratio between treated versus untreated (control) samples, designated as 1. Data are based on triplicate reactions of at least 3 biological samples.

Tissue staining, histology and immunohistochemistry

Whole mount X-gal staining, immunostaining and H&E staining were done using standard protocols as previously described (Mongan et al., 2008).

Transfection and luciferase assay

Cells seeded in 24-well tissue culture plates at 1×10^5 cells/well were grown for 16 h before transfection. Transfection was carried out with Lipofectamine Plus reagent (Invitrogen), using specific-firefly luciferase and CMV-renilla luciferase plasmids following the manufacturer's instructions. In some experiments, cells were co-transfected with Wnt3a and/or MAP3K1 expression vectors as described elsewhere (Belenkaya et al., 2008;Zhang et al., 2005), and in some others, the cells were treated with LiCl (20 mM) for 24 h. Twenty-four to 36 hours after transfection, cells were lysed and luciferase activities were determined using dual luciferase reporter kits (Promega).

Statistical and bioinformatics analyses

Microarray data were analyzed at gene level using statistical software R and the limma package of Bioconductor (Smyth, 2004) with custom CDF downloaded from BrainArray (Dai et al., 2005). Data pre-processing, including background correction and normalization, was performed using RMA. Array quality was assessed using the Array Quality Metrics package of Bioconductor (Kauffmann et al., 2009). Fold change was calculated by a separate linear model for each gene using limma package, and resulting *t*-statistics were modified using an intensity-based empirical Bayes method (IBMT) (Sartor et al., 2009b). Fold change of a gene is calculated as the ratio of average intensity of the gene in one genotype to the other. By convention, when the fold change is less than 1, the negative of its inverse is used.

Using IBMT p-values as the measure of statistical significance, functional enrichment analysis was performed using the logistic regression based LRpath methodology (Sartor et al., 2009a) as implemented in the R package CLEAN (Freudenberg et al., 2009). The gene list used in the functional enrichment analysis came from genes associated with Gene Ontology terms (Ashburner et al., 2000), KEGG pathways (Kanehisa et al., 2008), MSigDb database (Subramanian et al., 2005) and mammalian phenotypes (Blake et al., 2009). The statistical significance of gene list enrichment was determined based on the False Discovery

Rate (fdr) cut-off of 0.1. Genes that were both members of at least one statistically significant gene list and had IBMT p-value < 0.05 were considered to be differentially expressed.

The transcription factors (TF) whose target genes were enriched for differentially expressed genes were identified based on LRpath analysis of computationally derived lists of targets in MSigDb database (Subramanian et al., 2005) and in-house derived lists previously described in (Medvedovic et al., 2009) using the same fdr significance levels as for functional enrichment analysis.

Real-time RT-PCR and quantitative imaging data were subjected to statistical comparisons with Student's two-tailed paired *t test* and analysis of variance (ANOVA). Data represent the average ± s.d. from at least three independent experiments. Values of *p<0.05, ** p<0.01 and *** p<0.001 were considered statistically significant.

RESULTS

Eyelid leading edge (LE) and inner eyelid (IE) epithelia show distinct MAP3K1-regulated gene expression signatures

Mouse embryonic eyelid closure is a precisely orchestrated morphogenetic event, taking place within a narrow window of fetal development. The upper and lower eyelids are separated at E15.5, but they are fully closed and fused at E16.5 (Fig. 1A). In contrast to the wild type and heterozygous (*Map3k1*$^{+/\Delta KD}$) fetuses, in which the eyelids were closed at E16.5, the knockout (*Map3k1*$^{\Delta KD/\Delta KD}$) fetuses had their eyelids widely open. To identify the cells directly affected by MAP3K1 ablation, we examined MAP3K1 expression in the developing eyes by taking advantage of the *Map3k1*$^{\Delta KD}$ allele, which contains the bacterial β-galactosidase gene knocked-in into the *Map3k1* locus (Xia et al., 2000). After whole mount X-gal staining of the *Map3k1*$^{+/\Delta KD}$ fetuses, we measured β-gal expression as a surrogate for the expression of the endogenous MAP3K1 protein. The β-gal positive cells were most abundant in eyelid epithelium, and were almost undetectable in eyelid dermis and cornea (Fig. 1B). In addition, the β-gal positive cells were particularly enriched in the LE and IE epithelia, but were sparse in the epithelium of outer eyelid and skin. This pattern of expression prompted us to focus on the analysis of MAP3K1's functions in LE and IE epithelia.

Developmentally, the eyelid epithelium originates on E11-12 from the surface ectoderm, which folds to divide the outer and inner eyelid epithelium. After the initial division, the outer eyelid epithelium continues to differentiate towards epidermal lineages, and the IE epithelium is programmed to become conjunctiva (Wolosin et al., 2004). The LE, located at the crossroad junction of outer and IE epithelium, consists of a group of periderm cells that change their shape during eyelid closure. Because of their distinct characteristics and developmental fates, the LE and IE cells might be affected differently by MAP3K1 ablation. To identify the effects, we isolated LE and IE cells separately by LCM from E15.5 wild type and *Map3k1*$^{\Delta KD/\Delta KD}$ fetuses, the eyelids of which were morphologically indistinguishable at the optical microscopic level at this time point (Fig. 1B). We first examined MAP3K1 expression by real-time RT-PCR, using primers recognizing either *Map3k1* exon 18, specifically deleted, or β-gal, uniquely present, on the *Map3k1*$^{\Delta KD}$ allele. The level of β-gal mRNA was significantly lower in wild type than in *Map3k1*$^{\Delta KD/\Delta KD}$ embryos, whereas the level of *Map3k1* exon 18 was about 100-fold more abundant in wild type than in knockout cells (Fig. 1C). These results confirm the wild type and mutant *Map3k1* status at the mRNA level in the captured LE and IE epithelial cells.

We next examined global gene expression in these cells. We detected abundant mRNA for at least 15 cytokeratins and/or keratin-associated proteins, the majority of which were expressed equally in wild type and *Map3k1*$^{\Delta KD/\Delta KD}$ cells with only a few exceptions (Supplemental Table I). These observations suggest that the LCM captured wild type and *Map3k1*$^{\Delta KD/\Delta KD}$ samples have equivalent numbers of epithelial cells. Statistical analyses of the array data led to the identification of a total of 797 differentially expressed genes in LE and 1189 differentially expressed genes in IE epithelial cells (GEO repository, accession no. GSE39240). Unexpectedly, however, *Map3k1* was not one of the differentially expressed genes. We argued that because the *Map3k1*$^{\Delta KD}$ allele had only exons 15–21 deleted, the differential expression of these exons was masked when the full length mRNA was analyzed (Xia et al., 2000). To test this hypothesis, we examined the array signals generated by 84 oligo probes covering all 21 exons of the *Map3k1* gene. The probes for exons 1–14 produced signals with equal intensity in wild type and knockout cells, whereas probes for exons 15–17 detected significantly weaker signals in *Map3k1*$^{\Delta KD/\Delta KD}$ LE and IE cells and probes for exons 18–21 had poor hybridization quality (Fig. 2). Hence, the regions missing on the *Map3k1*$^{\Delta KD}$ allele had decreased expression in the knockout cells.

Bioinformatics analyses of the array data generate a list of statistically significant functional categories (supplemental Tables II–IX). The statistically significant functional categories associated with 12 dominant functional themes are listed in Table I. Differentially expressed genes associated with these functional categories are listed in Tables II – V, and Supplemental Tables X – XXVII. Strikingly, more than 95% of the differentially expressed genes in the LE are distinct from those in the IE epithelial cells, underscoring an exceptional temporal-spatial specificity of MAP3K1 in the developing eyelid.

MAP3K1 potentiates morphogenesis of the LE eyelid epithelium

Histological examination indicates that the LE cells of wild type fetuses undergo major morphological changes during embryonic eyelid closure, whereas those of *Map3k1*$^{\Delta KD/\Delta KD}$ fetuses do not (Zhang et al., 2003). Gene expression data provided a molecular basis to this observation, as they showed that the *Map3k1*$^{\Delta KD/\Delta KD}$ LE cells had decreased expression of genes involved in morphogenesis, actin re-organization, and migration (Table I). For example, compared to wild type cells, *Map3k1*$^{\Delta KD/\Delta KD}$ LE cells had less expression of Ephrin-A1 (*Efna1*), a crucial migration and morphogenetic factor, Palladin (*Palld*), responsible for organization of actin cytoskeleton, and Keratin 17 (*Krt17*) and α2-actin, markers for cell migration and epithelium-to-mesenchymal transformation (EMT) (Table II and Fig. 3A).

MAP3K1 has been shown to regulate B cell proliferation by mediating CD40 ligand-induced cyclin D2 expression (Gallagher et al., 2007), but its role in eyelid cell proliferation has not been reported. Our gene expression data identified a number of pro-proliferative genes expressed less abundantly in the knockout LE cells (Supplemental Table X). For example, relative to wild type cells, *Map3k1*$^{\Delta KD/\Delta KD}$ LE cells had reduced expression of fibroblast growth factor 7 (*Fgf7*), a major mitogenic and survival factor involved in proliferation and morphogenesis, and teratocarcinoma-derived growth factor 1 (*Tdgf1*), an epidermal growth factor-related protein with an essential role in cell proliferation (Table II and Fig. 3A). To evaluate whether cell proliferation was affected by MAP3K1, we examined the phosphorylation of histone H3, an event required for chromatin fiber decondensation, and chromosome compaction during mitosis. Phospho-H3 positive nuclei were observed in the epithelium and dermis of the E15.5 developing eyelids (Fig. 3B). While phospho-H3 positive nuclei were detected with similar frequencies in the eyelid dermis of all fetuses examined, they were clearly more abundant in the LE epithelium of wild type than *Map3k1*$^{\Delta KD/\Delta KD}$ fetuses.

H3 phosphorylation alone, however, is insufficient to support a role of MAP3K1 in proliferation, because besides being a marker for mitosis, H3 phosphorylation is also a common nucleosomal response to diverse stimuli associated with inducible transcriptional gene activation. To further evaluate the role of MAP3K1 in proliferation, we examined the array data for the expression of cell cycle markers (Supplemental Table XXVIII). Of the 127 cell cycle regulators, only 2 were found differentially expressed between wild type and *Map3k1*$^{\Delta KD/\Delta KD}$ LE cells, One is *Mcm2*, encoding minichromosome maintenance complex component 2 regulating S phase DNA replication initiation and elongation, and the other is *Abl1*, encoding a non-receptor tyrosine-protein kinase that coordinates actin remodeling and thereby cell growth and survival. The expression of *Mcm2* and *Abl1* was reduced by 45% and 36%, respectively, in the *Map3k1*$^{\Delta KD/\Delta KD}$ cells. On the other hand, *Mki67*, encoding an antigen identified by monoclonal antibody Ki-67, was expressed at similar level in wild type and *Map3k1*$^{\Delta KD/\Delta KD}$ LE cells. Ki-67 is known to be associated with and necessary for cellular proliferation. These results therefore suggest that although MAP3K1 enhances mitogen expression and H3 phosphorylation, it does not promote LE cell proliferation.

Crosstalk between MAP3K1 and morphogenetic signaling pathways

Mutations in Wnt, Sonic hedgehog (SHH), BMP/Activin B, FGF and EGF/TGFα amongst others cause mice to develop an EOB phenotype, suggesting that embryonic eyelid closure is regulated by multiple signaling pathways (Gage et al., 2008;Huang et al., 2009;Luetteke et al., 1993;Mine et al., 2005). Although how these signals interact to coordinate eyelid development is still an open question, we have shown, using genetic and molecular approaches, that MAP3K1 connects several of the pathways into a signaling network (Geh et al., 2011). In this network, EGF/TGFα activates MAP3K1 expression, while MAP3K1 in turn transduces Activin B signals to activate the JNK-c-Jun cascades. The present gene expression data suggest that Wnt and SHH are additional components of the network (Table III).

Wnt functions through activation of Frizzled receptors, leading to phosphorylation of Dishevelled (Dsh) proteins. Phosphorylated Dsh recruits the β-catenin destruction complex of axin/APC/GSK3β to the membrane, resulting in stabilization of β-catenin (Cadigan and Liu, 2006). Although MAP3K1 ablation did not affect the expression of different Wnt proteins or of their receptors and the members of the β-catenin destruction complex, it decreased the expression of six genes in LE and one gene in IE cells implicated in Wnt signaling (Table III and Supplemental Tables XV, XXII and XXIX). qRT-PCR confirmed that in the LE cells, MAP3K1 ablation reduced the expression of secreted frizzled-related protein 4 (*Sfrp4*), a soluble modulator of Wnt signaling, and in the IE cells, MAP3K1 ablation reduced the expression of the Wnt antagonist DKK2 (Fig. 4A).

Activation of Wnt leads to stabilization and subsequent translocation of β-catenin into the nucleus. Once inside the nucleus, β-catenin forms complexes with the DNA-binding transcription factor LEF/TCF to regulate Wnt-target genes (Cadigan and Liu, 2006). To evaluate whether MAP3K1 ablation affected the activity of Wnt, we examined wild type and *Map3k1*$^{\Delta KD/\Delta KD}$ for cellular localization of β-catenin. We found that in the eyelid epithelium of wild type fetuses, β-catenin was localized at the plasma membrane and cell-cell junctions, but in that of knockout fetuses it displayed a dispersed distribution in both cytosol and nucleus (Fig. 4B). To evaluate whether MAP3K1 ablation increased β-catenin activity, we introduced a luciferase reporter driven by the TCF/LEF DNA-binding sites into wild type and *Map3k1*$^{\Delta KD/\Delta KD}$ fibroblasts and measured luciferase expression (Brantjes et al., 2002). The results showed that Wnt3a expression induced luciferase activity by 3-fold in wild type cells and more than 10-fold in knockout cells (Fig. 4C). Similarly, while expression of wild type MAP3K1 had minimal effects, expression of kinase-inactive MAP3K1 {MAP3K1(KM)} significantly elevated TCF/LEF-luc activity in HEK293 cells

either untreated or treated with LiCl, which activates Wnt through the inhibition of GSK3 activity (Stambolic et al., 1996) (Fig. 4D).

Sonic hedgehog (SHH) is an important signal for EMT and crucial for embryonic eyelid closure (Huang et al., 2009;Lipinski et al., 2008;Young et al., 2000). This pathway is initiated by binding of SHH to its receptor PTCH1 that activates Smoothened. Smoothened in turn activates the GLI transcription factors to regulate downstream target gene expression (Riobo and Manning, 2007). We found that several members of this pathway, including *Gli2* and its target gene *Fgf9*, were down-regulated in *Map3k1*$^{\Delta KD/\Delta KD}$ LE epithelium (Pantalacci et al., 2008)(Table III). Using qRT-PCR, we confirmed that *Gli2* mRNA was less abundant in the LE epithelium of *Map3k1*$^{\Delta KD/\Delta KD}$ than in that of wild type (Fig. 4A), suggesting that MAP3K1 enhances SHH signaling. In summary, our results suggest that the MAP3K1-mediated signaling network has an expansive capacity, as it not only involves TGFα and Activin B signals, but also connects to Wnt and SHH signals.

MAP3K1 activates AP-2α, SRF and their pathways

To identify potential transcription factors acting downstream of MAP3K1, we determined whether the frequency of known transcription factor binding motifs was greater in the regulatory elements of genes differentially expressed in LE cells. MAP3K1 is a 196 kDa protein containing a N-terminal ubiquitin ligase domain and a C-terminal kinase domain (Lu et al., 2002;Xia et al., 2000). The MAP3K1-β-gal fusion protein derived from the *Map3k1*$^{\Delta KD}$ allele, while retaining the N-terminal domain, lacks the C-terminal domain. Given that *Map3k1*$^{\Delta KD/\Delta KD}$ and *Map3k1*$^{-/-}$ mice both exhibit EOB, it is likely that the kinase, but not the ubiquitin ligase activity is required for embryonic eyelid closure (Yujiri et al., 2000;Zhang et al., 2003). Previously, we have shown that the kinase activity of MAP3K1 is responsible for activation of the JNK-c-Jun cascades and the AP-1 transcription complex (Geh et al., 2011;Takatori et al., 2008). Our TF binding motifs analyses, however, did not find AP-1 target sequences over-represented among genes up-regulated by MAP3K1, suggesting that AP-1 was not directly responsible for MAP3K1-dependent gene expression. On the other hand, we identified AP-2 and SRF as two factors whose binding sites were highly enriched among genes up-regulated by MAP3K1 (Supplemental Table XXX).

The significant enrichment of AP-2 target genes, combined with the evidence that *AP-2α* knockout mice exhibit the EOB phenotype, led us to explore whether AP-2 was directly affected by MAP3K1 (West-Mays et al., 1999). The AP-2 family has five members: AP-2α, AP-2β, AP-2γ, AP-2δ, and AP-2ε, all possessing a basic helix–loop–helix (bHLH) domain at the C-terminus and a glutamine- and proline-rich domain at the N-terminus (Eckert et al., 2005). These AP-2 proteins form homodimers and heterodimers that bind to the palindromic sequence GCCN3GGC within multiple gene promoters (Hilger-Eversheim et al., 2000). In our array data, although the expression of other AP-2 members was unaffected by MAP3K1 ablation, the expression of AP-2α and AP-2β was reduced in *Map3k1*$^{\Delta KD/\Delta KD}$ cells (Table IV). Real time RT-PCR confirmed the reduction of *Ap2a* expression by MAP3K1 ablation in LE and IE cells (Fig. 5A). A well recognized function of AP-2α is the modulation of epidermal lineage specification and hair follicle gene expression (Panteleyev et al., 2001;Wang et al., 2008). Accordingly, the IE and LE cells of the *Map3k1*$^{\Delta KD/\Delta KD}$ had lower levels of hair follicle gene expression than those of the wild type fetuses (Table V), suggesting that the MAP3K1-AP-2 axis may be involved in hair follicle gene expression.

The SRF is a transcription factor that binds to CC(AT)6GG DNA sequences, as part of the serum response elements (SREs) located in the promoters of target gene (Shaw et al., 1989). Because our expression data showed that MAP3K1 ablation did not alter SRF expression (Table IV), we tested whether MAP3K1 could affect SRF activity (Soh et al., 1999). We

transfected HEK293 cells with luciferase reporter vectors responsive to transcription factors, including AP-1, SMAD and SRF; in some experiments, we co-transfected plasmids for active MAP3K1. We found that active MAP3K1 did not affect SMAD-dependent luciferase activity (SBE-luc), but it significantly stimulated SRF- as well as AP-1-dependent activity (Fig. 5B). SRF binding motifs are frequent in the promoter of genes controlling cell motility, such as *Fgf7*, *α2-actin*, *Transgelin* and *keratin 17*, underscoring the involvement of the MAP3K1-SRF axis in LE cell migration (Table VI).

Differentiation programs in LE and IE epithelium are affected by MAP3K1

An unexpected finding from the gene expression data was that MAP3K1 affected the transcription of multiple lineage differentiation genes (Table V). Specifically, it inhibited crystallin expression in LE epithelium, and skeletal muscle genes in IE epithelium, and induced hair follicle genes in both LE and IE epithelium.

Although crystallins are known as structural proteins of the lens and cornea responsible for the transparency of the eye, crystallin gene transcripts were detected in the LE epithelial cells. At least 10 crystallin mRNAs were significantly more abundant in knockout than wild type LE cells. RT-PCR confirmed that three of these, *Crystallinba1*, *Crystallinba2* and *Crystallingn*, were expressed at 15–20-fold higher levels in the knockout cells (Fig. 6A). PAX6 is a master transcription regulator of crystalline genes (Graw, 2009;Grindley et al., 1995;shery-Padan et al., 2000). However, MAP3K1 ablation did not alter either the expression of members of the *Pax6* family, or the expression of PAX6 co-factors, including the large Maf proteins, *Mafa* and *Mafb*, *Pax2*, *Prox1*, *Six3*, *Pitx3*, *FoxE3*, *Sox1* and *Sox2*, and *Otx2* (Cvekl and Duncan, 2007) (Supplemental Tables XXXII and XXXIII). On the other hand, we found that MAP3K1 ablation caused down-regulation of FGF and up-regulation of Wnt signaling, whereas FGF and Wnt may in turn regulate crystallin gene transcription (Chen et al., 2006) (Supplemental Tables XXIX and XXXIV).

A number of skeletal muscle gene transcripts were expressed at higher levels in *Map3k1*$^{\Delta KD/\Delta KD}$ than in wild type IE epithelial cells (Table V). qRT-PCR showed that five genes in this category, including actin α1 (*Acta1*), fast skeletal phosphorylatable myosin light chain (*Mlcpf*), myosin binding protein C (*Myfopc1*), troponin I type 2 (*Tnni2*) and troponin T3 (*Tnnt3*), were expressed more abundantly in the knockout cells (Fig. 6B). Although these observations implied that MAP3K1 repressed skeletal muscle differentiation in the IE epithelium, immunohistochemical studies detected no trace of skeletal muscle (SK myosin) or smooth muscle (α-SM actin) proteins in the IE of fetuses at various embryonic stages of either genotypes (Fig. 6C). Immunohistochemistry detected instead inferior tarsal muscles (α-SM actin positive) in the lower eyelids adjacent to the IE epithelium and the bundle of skeletal muscles (α-SM actin and SK myosin positive) located in the middle of the developing eyelids. Both muscles displayed aberrant differentiation patterns in the *Map3k1*$^{\Delta KD/\Delta KD}$ fetuses. Based on these observations, we speculate that the IE epithelial cells captured by LCM might be contaminated with nearby myocytes. This is unlikely to be the case, however, because our gene expression analysis of cultured keratinocytes from wild type and *Map3k1*$^{\Delta KD/\Delta KD}$ mice showed that loss of MAP3K1 led to the increased expression of a number of muscle-specific genes (Deng et al., 2006) (Table VII). Some of the genes, such as *Mlcpf* and *Acta1*, were affected by MAP3K1 ablation similarly in keratinocytes and IE epithelium. Repression of muscle-specific gene transcription therefore seems to be an intrinsic property of MAP3K1 in epithelial cells.

Lastly, in both LE and IE epithelial cells, we detected the expression of genes implicated in hair follicle development, with lower levels in *Map3k1*$^{\Delta KD/\Delta KD}$ than in wild type (Table V and Fig. 6D). MAP3K1 ablation decreased the expression of keratin 17, a hair follicle and epidermal appendage marker; it also down-regulated the expression of keratins 25 and 27,

which are type I intermediate filaments, and keratins 71 and 73, which are type II intermediate filaments, and trichohyalin (*Tchh*) and hair keratin-associated proteins (KRTAP), which are intermediate filament-associated proteins specifically implicated in inner root sheath of hair follicles(Gritli-Linde et al., 2007;Strnad et al., 2011). These observations led us to ask whether MAP3K1 ablation affected the development and structure of hair follicle and epidermis. Microscopic examination of representative dorsal haired skin longitudinal sections of postnatal day 1 (P1) revealed no overt structural changes in *Map3k1*$^{\Delta KD/\Delta KD}$ hair follicles, epidermis, or dermis when compared to controls (Fig. 6E). Additionally, no grossly appreciable skin or coat abnormalities are present in knockout mice. Whether the altered gene expression led to discrete ultrastructural changes in hair follicle components was not determined.

DISCUSSION

Cell heterogeneity and the temporal-spatial nature of gene regulation constitute a major challenge to study gene expression in developing tissues. Our initial attempt to microarray studies used whole eyelid tissues macro dissected from wild type and *Map3k1*$^{\Delta KD/\Delta KD}$ fetuses, which generated dispersed expression patterns with no outstanding signatures. We then modified the strategy by using LCM to capture a highly enriched cell population. The LCM samples exhibit abundant expression of epithelial-specific genes, but they also have a few detectable mesenchymal markers, such as *Vimentin* and *Fgf7*. Because these markers are detected also in the *in vitro* cultured keratinocytes that do not contain mesenchymal cells (Supplemental Table XXXV), their presence in the LCM samples may not be a sign of mesenchymal cell contamination. Nevertheless, the LCM samples have significantly improved array quality, resulting in reliable gene expression signatures with considerably reduced noise and variability. By integrating LCM with expression arrays, we identified gene transcription signatures in subgroups of eyelid cells in which MAP3K1 is most abundantly expressed. Strikingly, the transcriptome data reveal an extremely small overlap in MAP3K1 affected genes between LE and IE, suggesting that even though MAP3K1 is similarly expressed, it has distinct spatial-temporal activities. In the LE, the subset cells most relevant to embryonic eyelid closure, MAP3K1 is shown to regulate actin cytoskeleton, EMT and morphogenesis. Since these signatures are identified at E15.5, a developmental stage prior to eyelid closure, they likely characterize molecular and cellular events through which MAP3K1 controls embryonic eyelid closure.

Results from the current work have extended our view of the signaling properties of MAP3K1, because they suggest that MAP3K1 is not only the downstream transducer of the TGFα/EGF and TGFβ/activin B signals, but can also act as an upstream modulator of Wnt and SHH signals. How MAP3K1 establishes a crosstalk with these pathways is not understood at the molecular level, with many possible direct and indirect mechanisms. On the one hand, MAP3K1 may activate the JNK cascades to affect directly the expression and activity of Wnt and SHH; on the other hand, it may act through an intermediary, such as FGF, or a biological process, such as cell migration, to influence indirectly Wnt and SHH (Grotewold and Ruther, 2002;Huang et al., 2009;Weston et al., 2003). Our results suggest that MAP3K1 may have more expansive signaling properties than previously thought, as it appears to interact with many developmental pathways to coordinate the morphogenetic programs in the LE cells.

The gene expression data suggest that MAP3K1 attenuates Wnt signaling, a conclusion consistent with the notion that Wnt inhibition is necessary for embryonic eyelid closure and with the observation that knocking out the Wnt antagonist DKK2 results in EOB (Gage et al., 2008). In the LE cells of the *Map3k1*$^{\Delta KD/\Delta KD}$ fetuses, however, we note that β-catenin is not highly accumulated in the nucleus but rather is dispersed throughout the cells. These

observations raise a possibility that MAP3K1 ablation causes just a slight disturbance of the Wnt signaling. While this possibility is yet to be tested, a recent study showed an opposite effect of MAP3K1 on Wnt signaling. It was observed that in colorectal cancer cells MAP3K1 interacted with the Wnt negative regulator Axin1 and caused the activation of β-catenin and Wnt target genes (Sue et al., 2010). This function depended on MAP3K1's E3 ubiquitin ligase activity mediated through its RING domain, and was independent of its kinase activity, required for embryonic eyelid closure. It is hence possible that through differential usage of its functional domains, MAP3K1 can either activate or repress Wnt signaling in a cell type- and biological process-dependent manner.

We have previously shown that MAP3K1 is required for optimal c-Jun N-terminal phosphorylation as well as AP-1 activity in LE cells (Geh et al., 2011;Takatori et al., 2008). In agreement with these findings, we find that MAP3K1 stimulates AP-1 activity in HEK293 cells. It has long been held that MAP3K1 regulates eyelid closure through activation of c-Jun and AP-1 and their downstream genes; however, the genetic evidence challenges this idea. Genetic studies have shown that although c-Jun expression is essential for embryonic eyelid closure, its N-terminal phosphorylation is dispensable for this function (Behrens et al., 1999;Li et al., 2003;Zenz and Wagner, 2006). Our TF binding site enrichment analyses support the genetic evidence. The enrichment analysis results show that AP-1 binding sites are not found among the genes up-regulated in wild type LE cells, suggesting that c-Jun/AP-1 activation by MAP3K1 either makes trivial contributions to eyelid closure or contributes indirectly by facilitating the functions of other transcription factors. On the other hand, binding sites for AP-2 and SRF are highly enriched among genes up-regulated by MAP3K1; correspondingly, MAP3K1 is required for optimal AP-2 expression and SRF activity. These observations are consistent with the fact that both AP-2α and SRF are implicated in eyelid development, as shown by the EOB phenotype of their knockout mice (Verdoni et al., 2010;West-Mays et al., 1999). The AP-2 and SRF are known to play crucial roles in differentiation, therefore, their dysregulation may be responsible for aberrant differentiation of epithelium, hair follicles, muscle and lens placode in the *Map3k1*$^{\Delta KD/\Delta KD}$ cells (Aline and Sotiropoulos, 2012;Wang et al., 2008;Wenke and Bosserhoff, 2010;West-Mays et al., 1999). Taken together, our results suggest that eyelid morphogenesis is regulated by a novel mechanism in which MAP3K1 acts through AP2 and SRF to control gene expression.

The gene expression data also reveal the unique signatures of MAP3K1 in lineage-specific gene transcription in the LE and IE epithelium. Specifically, there is a clear inverse relationship between MAP3K1 and transcription of crystallin genes in LE cells and skeletal muscle genes in IE cells. In addition, there is a parallel relationship between MAP3K1 and transcription of hair follicle genes in both LE and IE epithelium. An important caveat is that gene transcription signatures may not accurately reflect functional endpoints, because there is scant evidence to indicate that MAP3K1 ablation alters any of the differentiation programs at the protein level. One possible explanation is that the developing cells have powerful post-transcriptional mechanisms, such as non-coding RNAs, to control differentiation. These machineries will allow efficient translation of specific mRNA in permissive cells, but impair translation in non-permissive cells.

Collectively, this work provides an example illustrating the use of LCM, gene knockout system and expression array to gain mechanistic understanding of gene functions in developmental tissues. With this approach, we have identified novel molecular and signaling pathways through which MAP3K1 regulates embryonic eyelid closure.

Supplementary Material

Refer to Web version on PubMed Central for supplementary material.

Acknowledgments

We wish to thank Drs. Xinhua Lin and Xiaofang Tang (Cincinnati Children's Hospital Medical Center), and Drs. Jinsong Zhang and Yujin Zhang (University of Cincinnati) for plasmids and reagents and Dr. Alvaro Puga (University of Cincinnati) for a critical reading of the manuscript. The work is supported in part by funding from NIH, NEI R01-EY15227 (Y.X.), NIEHS T32 ES07250 and F31EY019458 (E.G.), NIEHS P30-ES006096 (Y.X., M.M. and S.H.) and the Key Research and Development Program project grant 2008C14097 from Zhejiang Province, China (X.Z.).

References

Aguilera C, Nakagawa K, Sancho R, Chakraborty A, Hendrich B, Behrens A. c-Jun N-terminal phosphorylation antagonises recruitment of the Mbd3/NuRD repressor complex. Nature. 2011; 469:231–235. [PubMed: 21196933]

Aline G, Sotiropoulos A. Srf: A key factor controlling skeletal muscle hypertrophy by enhancing the recruitment of muscle stem cells. Bioarchitecture. 2012; 2:88–90. [PubMed: 22880147]

Ashburner M, Ball CA, Blake JA, Botstein D, Butler H, Cherry JM, Davis AP, Dolinski K, Dwight SS, Eppig JT, Harris MA, Hill DP, Issel-Tarver L, Kasarskis A, Lewis S, Matese JC, Richardson JE, Ringwald M, Rubin GM, Sherlock G. Gene ontology: tool for the unification of biology. The Gene Ontology Consortium. Nat Genet. 2000; 25:25–29. [PubMed: 10802651]

Behrens A, Sibilia M, Wagner EF. Amino-terminal phosphorylation of c-Jun regulates stress-induced apoptosis and cellular proliferation. Nat Genet. 1999; 21:326–329. [PubMed: 10080190]

Belenkaya TY, Wu Y, Tang X, Zhou B, Cheng L, Sharma YV, Yan D, Selva EM, Lin X. The retromer complex influences Wnt secretion by recycling wntless from endosomes to the trans-Golgi network. Dev Cell. 2008; 14:120–131. [PubMed: 18160348]

Blake JA, Bult CJ, Eppig JT, Kadin JA, Richardson JE. The Mouse Genome Database genotypes::phenotypes. Nucleic Acids Res. 2009; 37:D712–D719. [PubMed: 18981050]

Brantjes H, Barker N, van EJ, Clevers H. TCF: Lady Justice casting the final verdict on the outcome of Wnt signalling. Biol Chem. 2002; 383:255–261. [PubMed: 11934263]

Cadigan KM, Liu YI. Wnt signaling: complexity at the surface. J Cell Sci. 2006; 119:395–402. [PubMed: 16443747]

Chen Y, Stump RJ, Lovicu FJ, McAvoy JW. A role for Wnt/planar cell polarity signaling during lens fiber cell differentiation? Semin Cell Dev Biol. 2006; 17:712–725. [PubMed: 17210263]

Craig EA, Stevens MV, Vaillancourt RR, Camenisch TD. MAP3Ks as central regulators of cell fate during development. Dev Dyn. 2008; 237:3102–3114. [PubMed: 18855897]

Cvekl A, Duncan MK. Genetic and epigenetic mechanisms of gene regulation during lens development. Prog Retin Eye Res. 2007; 26:555–597. [PubMed: 17905638]

Dai M, Wang P, Boyd AD, Kostov G, Athey B, Jones EG, Bunney WE, Myers RM, Speed TP, Akil H, Watson SJ, Meng F. Evolving gene/transcript definitions significantly alter the interpretation of GeneChip data. Nucleic Acids Res. 2005; 33:e175. [PubMed: 16284200]

Davis RJ. Transcriptional regulation by MAP kinases. Mol Reprod Dev. 1995; 42:459–67. [PubMed: 8607977]

Deng M, Chen WL, Takatori A, Peng Z, Zhang L, Mongan M, Parthasarathy R, Sartor M, Miller M, Yang J, Su B, Kao WW, Xia Y. A role for the mitogen-activated protein kinase kinase kinase 1 in epithelial wound healing. Mol Biol Cell. 2006; 17:3446–3455. [PubMed: 16760432]

Eckert D, Buhl S, Weber S, Jager R, Schorle H. The AP-2 family of transcription factors. Genome Biol. 2005; 6:246. [PubMed: 16420676]

Findlater GS, McDougall RD, Kaufman MH. Eyelid development, fusion and subsequent reopening in the mouse. J Anat. 1993; 183:121–9. [PubMed: 8270467]

Freudenberg JM, Joshi VK, Hu Z, Medvedovic M. CLEAN: CLustering Enrichment ANalysis. BMC Bioinformatics. 2009; 10:234. [PubMed: 19640299]

Gage PJ, Qian M, Wu D, Rosenberg KI. The canonical Wnt signaling antagonist DKK2 is an essential effector of PITX2 function during normal eye development. Dev Biol. 2008; 317:310–324. [PubMed: 18367164]

Gallagher E, Enzler T, Matsuzawa A, nzelon-Mills A, Otero D, Holzer R, Janssen E, Gao M, Karin M. Kinase MEKK1 is required for CD40-dependent activation of the kinases Jnk and p38, germinal center formation, B cell proliferation and antibody production. Nat Immunol. 2007; 8:57–63. [PubMed: 17143273]

Gao M, Labuda T, Xia Y, Gallagher E, Fang D, Liu YC, Karin M. Jun turnover is controlled through JNK-dependent phosphorylation of the E3 ligase Itch. Science. 2004; 306:271–275. [PubMed: 15358865]

Geh E, Meng Q, Mongan M, Wang J, Takatori A, Zheng Y, Puga A, Lang RA, Xia Y. Mitogen-activated protein kinase kinase kinase 1 (MAP3K1) integrates developmental signals for eyelid closure. Proc Natl Acad Sci U S A. 2011; 108:17349–17354. [PubMed: 21969564]

Graw J. Genetics of crystallins: cataract and beyond. Exp Eye Res. 2009; 88:173–189. [PubMed: 19007775]

Grindley JC, Davidson DR, Hill RE. The role of Pax-6 in eye and nasal development. Development. 1995; 121:1433–1442. [PubMed: 7789273]

Gritli-Linde A, Hallberg K, Harfe BD, Reyahi A, Kannius-Janson M, Nilsson J, Cobourne MT, Sharpe PT, McMahon AP, Linde A. Abnormal hair development and apparent follicular transformation to mammary gland in the absence of hedgehog signaling. Dev Cell. 2007; 12:99–112. [PubMed: 17199044]

Grotewold L, Ruther U. The Wnt antagonist Dickkopf-1 is regulated by Bmp signaling and c-Jun and modulates programmed cell death. EMBO J. 2002; 21:966–975. [PubMed: 11867524]

Hilger-Eversheim K, Moser M, Schorle H, Buettner R. Regulatory roles of AP-2 transcription factors in vertebrate development, apoptosis and cell-cycle control. Gene. 2000; 260:1–12. [PubMed: 11137286]

Hu Q, Guo C, Li Y, Aronow BJ, Zhang J. LMO7 mediates cell-specific activation of the Rho-myocardin-related transcription factor-serum response factor pathway and plays an important role in breast cancer cell migration. Mol Cell Biol. 2011; 31:3223–3240. [PubMed: 21670154]

Huang J, Dattilo LK, Rajagopal R, Liu Y, Kaartinen V, Mishina Y, Deng CX, Umans L, Zwijsen A, Roberts AB, Beebe DC. FGF-regulated BMP signaling is required for eyelid closure and to specify conjunctival epithelial cell fate. Development. 2009; 136:1741–1750. [PubMed: 19369394]

Kanehisa M, Araki M, Goto S, Hattori M, Hirakawa M, Itoh M, Katayama T, Kawashima S, Okuda S, Tokimatsu T, Yamanishi Y. KEGG for linking genomes to life and the environment. Nucleic Acids Res. 2008; 36:D480–D484. [PubMed: 18077471]

Kauffmann A, Gentleman R, Huber W. arrayQualityMetrics--a bioconductor package for quality assessment of microarray data. Bioinformatics. 2009; 25:415–416. [PubMed: 19106121]

Labuda T, Christensen JP, Rasmussen S, Bonnesen B, Karin M, Thomsen AR, Odum N. MEK kinase 1 is a negative regulator of virus-specific CD8(+) T cells. Eur J Immunol. 2006; 36:2076–2084. [PubMed: 16761309]

Li G, Gustafson-Brown C, Hanks SK, Nason K, Arbeit JM, Pogliano K, Wisdom RM, Johnson RS. c-Jun Is Essential for Organization of the Epidermal Leading Edge. Dev Cell. 2003; 4:865–877. [PubMed: 12791271]

Lipinski RJ, Hutson PR, Hannam PW, Nydza RJ, Washington IM, Moore RW, Girdaukas GG, Peterson RE, Bushman W. Dose- and route-dependent teratogenicity, toxicity, and pharmacokinetic profiles of the hedgehog signaling antagonist cyclopamine in the mouse. Toxicol Sci. 2008; 104:189–197. [PubMed: 18411234]

Lu Z, Xu S, Joazeiro C, Cobb MH, Hunter T. The PHD domain of MEKK1 acts as an E3 ubiquitin ligase and mediates ubiquitination and degradation of ERK1/2. Mol Cell. 2002; 9:945–956. [PubMed: 12049732]

Luetteke NC, Qiu TH, Peiffer RL, Oliver P, Smithies O, Lee DC. TGF alpha deficiency results in hair follicle and eye abnormalities in targeted and waved-1 mice. Cell. 1993; 73:263–78. [PubMed: 8477445]

Medvedovic M, Gear R, Freudenberg JM, Schneider J, Bornschein R, Yan M, Mistry MJ, Hendrix H, Karyala S, Halbleib D, Heffelfinger S, Clegg DJ, Anderson MW. Influence of Fatty Acid Diets on Gene Expression in Rat Mammary Epithelial Cells. Physiol Genomics. 2009

Minamino T, Yujiri T, Terada N, Taffet GE, Michael LH, Johnson GL, Schneider MD. MEKK1 is essential for cardiac hypertrophy and dysfunction induced by Gq. Proc Natl Acad Sci U S A. 2002; 99:3866–3871. [PubMed: 11891332]

Mine N, Iwamoto R, Mekada E. HB-EGF promotes epithelial cell migration in eyelid development. Development. 2005; 132:4317–4326. [PubMed: 16141218]

Mongan M, Tan Z, Chen L, Peng Z, Dietsch M, Su B, Leikauf G, Xia Y. Mitogen-activated protein kinase kinase kinase 1 protects against nickel-induced acute lung injury. Toxicol Sci. 2008; 104:405–411. [PubMed: 18467339]

Pantalacci S, Prochazka J, Martin A, Rothova M, Lambert A, Bernard L, Charles C, Viriot L, Peterkova R, Laudet V. Patterning of palatal rugae through sequential addition reveals an anterior/posterior boundary in palatal development. BMC Dev Biol. 2008; 8:116. [PubMed: 19087265]

Panteleyev AA, Jahoda CA, Christiano AM. Hair follicle predetermination. J Cell Sci. 2001; 114:3419–3431. [PubMed: 11682602]

Riobo NA, Manning DR. Pathways of signal transduction employed by vertebrate Hedgehogs. Biochem J. 2007; 403:369–379. [PubMed: 17419683]

Sartor MA, Leikauf GD, Medvedovic M. LRpath: a logistic regression approach for identifying enriched biological groups in gene expression data. Bioinformatics. 2009a; 25:211–217. [PubMed: 19038984]

Sartor MA, Leikauf GD, Medvedovic M. LRpath: a logistic regression approach for identifying enriched biological groups in gene expression data. Bioinformatics. 2009b; 25:211–217. [PubMed: 19038984]

Schnekenburger M, Talaska G, Puga A. Chromium cross-links histone deacetylase 1-DNA methyltransferase 1 complexes to chromatin, inhibiting histone-remodeling marks critical for transcriptional activation. Mol Cell Biol. 2007; 27:7089–7101. [PubMed: 17682057]

Shaw PE, Schroter H, Nordheim A. The ability of a ternary complex to form over the serum response element correlates with serum inducibility of the human c-fos promoter. Cell. 1989; 56:563–572. [PubMed: 2492906]

shery-Padan R, Marquardt T, Zhou X, Gruss P. Pax6 activity in the lens primordium is required for lens formation and for correct placement of a single retina in the eye. Genes Dev. 2000; 14:2701–2711. [PubMed: 11069887]

Smyth GK. Linear models and empirical bayes methods for assessing differential expression in microarray experiments. Stat Appl Genet Mol Biol. 2004; 3 Article3.

Soh JW, Lee EH, Prywes R, Weinstein IB. Novel roles of specific isoforms of protein kinase C in activation of the c-fos serum response element. Mol Cell Biol. 1999; 19:1313–1324. [PubMed: 9891065]

Stambolic V, Ruel L, Woodgett JR. Lithium inhibits glycogen synthase kinase-3 activity and mimics wingless signalling in intact cells. Curr Biol. 1996; 6:1664–1668. [PubMed: 8994831]

Strnad P, Usachov V, Debes C, Grater F, Parry DA, Omary MB. Unique amino acid signatures that are evolutionarily conserved distinguish simple-type, epidermal and hair keratins. J Cell Sci. 2011; 124:4221–4232. [PubMed: 22215855]

Subramanian A, Tamayo P, Mootha VK, Mukherjee S, Ebert BL, Gillette MA, Paulovich A, Pomeroy SL, Golub TR, Lander ES, Mesirov JP. Gene set enrichment analysis: a knowledge-based approach for interpreting genome-wide expression profiles. Proc Natl Acad Sci U S A. 2005; 102:15545–15550. [PubMed: 16199517]

Sue NS, Mahmoudi T, Li VS, Hatzis P, Boersema PJ, Mohammed S, Heck AJ, Clevers H. MAP3K1 functionally interacts with Axin1 in the canonical Wnt signalling pathway. Biol Chem. 2010; 391:171–180. [PubMed: 20128690]

Takatori A, Geh E, Chen L, Zhang L, Meller J, Xia Y. Differential transmission of MEKK1 morphogenetic signals by JNK1 and JNK2. Development. 2008; 135:23–32. [PubMed: 18032450]

Venuprasad K, Elly C, Gao M, Salek-Ardakani S, Harada Y, Luo JL, Yang C, Croft M, Inoue K, Karin M, Liu YC. Convergence of Itch-induced ubiquitination with MEKK1-JNK signaling in Th2 tolerance and airway inflammation. J Clin Invest. 2006; 116:1117–1126. [PubMed: 16557301]

Verdoni AM, Ikeda S, Ikeda A. Serum response factor is essential for the proper development of skin epithelium. Mamm Genome. 2010; 21:64–76. [PubMed: 20047077]

Wang X, Pasolli HA, Williams T, Fuchs E. AP-2 factors act in concert with Notch to orchestrate terminal differentiation in skin epidermis. J Cell Biol. 2008; 183:37–48. [PubMed: 18824566]

Wenke AK, Bosserhoff AK. Roles of AP-2 transcription factors in the regulation of cartilage and skeletal development. FEBS J. 2010; 277:894–902. [PubMed: 20050923]

West-Mays JA, Zhang J, Nottoli T, Hagopian-Donaldson S, Libby D, Strissel KJ, Williams T. AP-2alpha transcription factor is required for early morphogenesis of the lens vesicle. Dev Biol. 1999; 206:46–62. [PubMed: 9918694]

Weston CR, Wong A, Hall JP, Goad ME, Flavell RA, Davis RJ. JNK initiates a cytokine cascade that causes Pax2 expression and closure of the optic fissure. Genes Dev. 2003; 17:1271–1280. [PubMed: 12756228]

Wolosin JM, Budak MT, Akinci MA. Ocular surface epithelial and stem cell development. Int J Dev Biol. 2004; 48:981–991. [PubMed: 15558489]

Xia Y, Makris C, Su B, Li E, Yang J, Nemerow GR, Karin M. MEK kinase 1 is critically required for c-Jun N-terminal kinase activation by proinflammatory stimuli and growth factor-induced cell migration. Proc Natl Acad Sci U S A. 2000; 97:5243–8. [PubMed: 10805784]

Xia Y, Wu Z, Su B, Murray B, Karin M. JNKK1 organizes a MAP kinase module through specific and sequential interactions with upstream and downstream components mediated by its amino-terminal extension. Genes Dev. 1998; 12:3369–81. [PubMed: 9808624]

Yan M, Dai T, Deak JC, Kyriakis JM, Zon LI, Woodgett JR, Templeton DJ. Activation of stress-activated protein kinase by MEKK1 phosphorylation of its activator SEK1. Nature. 1994; 372:798–800. [PubMed: 7997270]

Young DL, Schneider RA, Hu D, Helms JA. Genetic and teratogenic approaches to craniofacial development. Crit Rev Oral Biol Med. 2000; 11:304–317. [PubMed: 11021632]

Yujiri T, Sather S, Fanger GR, Johnson GL. Role of MEKK1 in cell survival and activation of JNK and ERK pathways defined by targeted gene disruption. Science. 1998; 282:1911–4. [PubMed: 9836645]

Yujiri T, Ware M, Widmann C, Oyer R, Russell D, Chan E, Zaitsu Y, Clarke P, Tyler K, Oka Y, Fanger GR, Henson P, Johnson GL. MEK kinase 1 gene disruption alters cell migration and c-Jun NH2-terminal kinase regulation but does not cause a measurable defect in NF-kappa B activation. Proc Natl Acad Sci U S A. 2000; 97:7272–7. [PubMed: 10852963]

Zenz R, Wagner EF. Jun signalling in the epidermis: From developmental defects to psoriasis and skin tumors. Int J Biochem Cell Biol. 2006; 38:1043–1049. [PubMed: 16423552]

Zhang L, Deng M, Parthasarathy R, Wang L, Mongan M, Molkentin JD, Zheng Y, Xia Y. MEKK1 transduces activin signals in keratinocytes to induce actin stress fiber formation and migration. Mol Cell Biol. 2005; 25:60–65. [PubMed: 15601830]

Zhang L, Wang W, Hayashi Y, Jester JV, Birk DE, Gao M, Liu CY, Kao WW, Karin M, Xia Y. A role for MEK kinase 1 in TGF-beta/activin-induced epithelium movement and embryonic eyelid closure. Embo J. 2003; 22:4443–4454. [PubMed: 12941696]

HIGHLIGHTS

- Uncover MAP3K1-dependent transcriptom in specific subsets of developing cells
- Expression signatures reveal patio-temporal specificity of MAP3K1 in development
- MAP3K1 can module Wnt and Shh signaling in the eyelid closure process
- AP2α and SRF are novel downstream transcription factors of MAP3K1 signaling

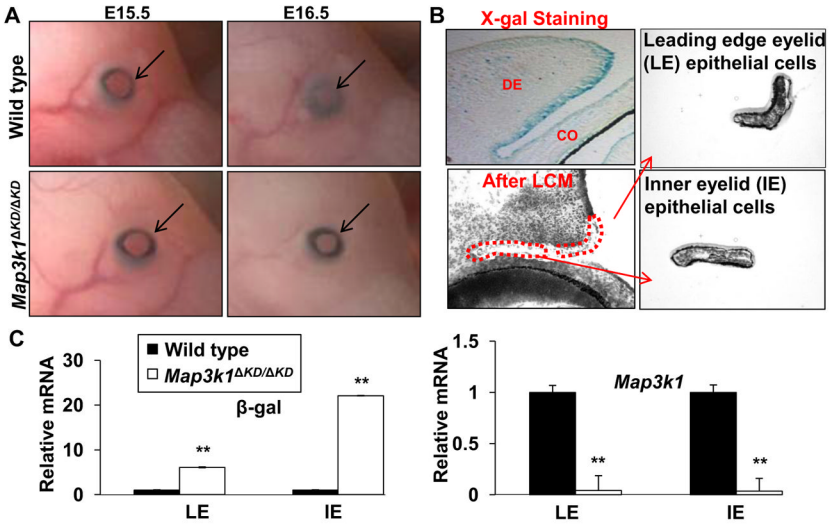

Figure 1. MAP3K1 expression and function in developing eyelids

(A) Photographs show the developing eyes of wild type and *Map3k1*$^{\Delta KD/\Delta KD}$ fetuses at E15.5 and E16.5. Arrows point at developing eyelids, showing that the eyelids are fully open in E15.5 fetuses of both genotypes, while they are closed in E16.5 wild type, but not knockout fetuses. (B) X-gal stained *Map3k1* heterozygous fetuses (*Map3k1*$^{+/\Delta KD}$) at E15.5 were sectioned and photographed (upper left). Pictures were taken before (upper left) and after (lower left) LCM, and the captured leading edge eyelid (LE) (upper right) and inner eyelid (IE) (lower right) epithelium. (C) Total RNA from LE and IE epithelium were subjected to qRT-PCR using primers for the kinase domain of *Map3k1* (*Map3k1*) and *β-gal* as indicated. Relative expression was calculated based on that of *Gapdh* in each sample, and compared to the expression in wild type cells, set as 1. The results are shown as mean ± SD from at least 3 samples of each genotype and triplicate PCR of each sample. Statistic analyses were done by Student *t-test,* $^{**}p < 0.01$ is considered significant. LE, leading edge eyelid, IE, inner eyelid, DE, dermis, CO, cornea.

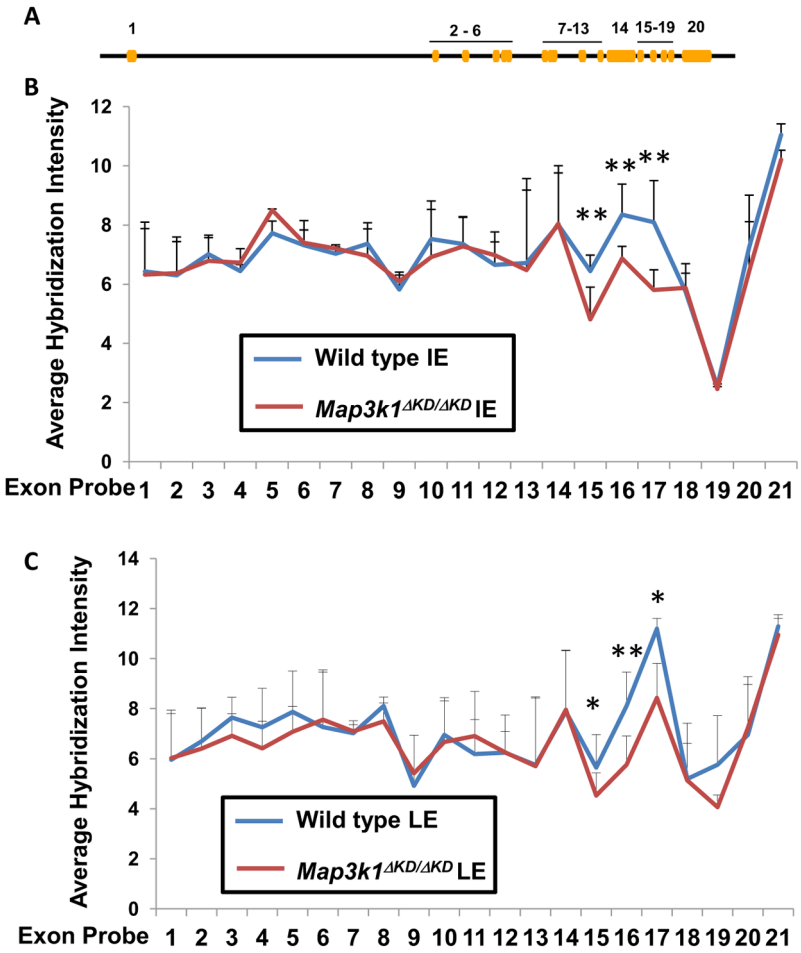

Figure 2. The *Map3k1* mRNA levels in wild type and *Map3k1*$^{\Delta KD/\Delta KD}$ cells

(A) A schematic illustration of *Map3k1* genome map. The hybridization signal intensity of *Map3k1* exon probes with RNA isolated from wild type and *Map3k1*$^{\Delta KD/\Delta KD}$ (B) IE, and (C) LE epithelium. Data represent the average intensity of the probes for each exon. Statistic analyses are done by student *t-test* comparing the intensity in wild type and *Map3k1*$^{\Delta KD/\Delta KD}$. *p<0.05 and **p<0.01 are considered significant. LE, leading edge eyelid, IE, inner eyelid.

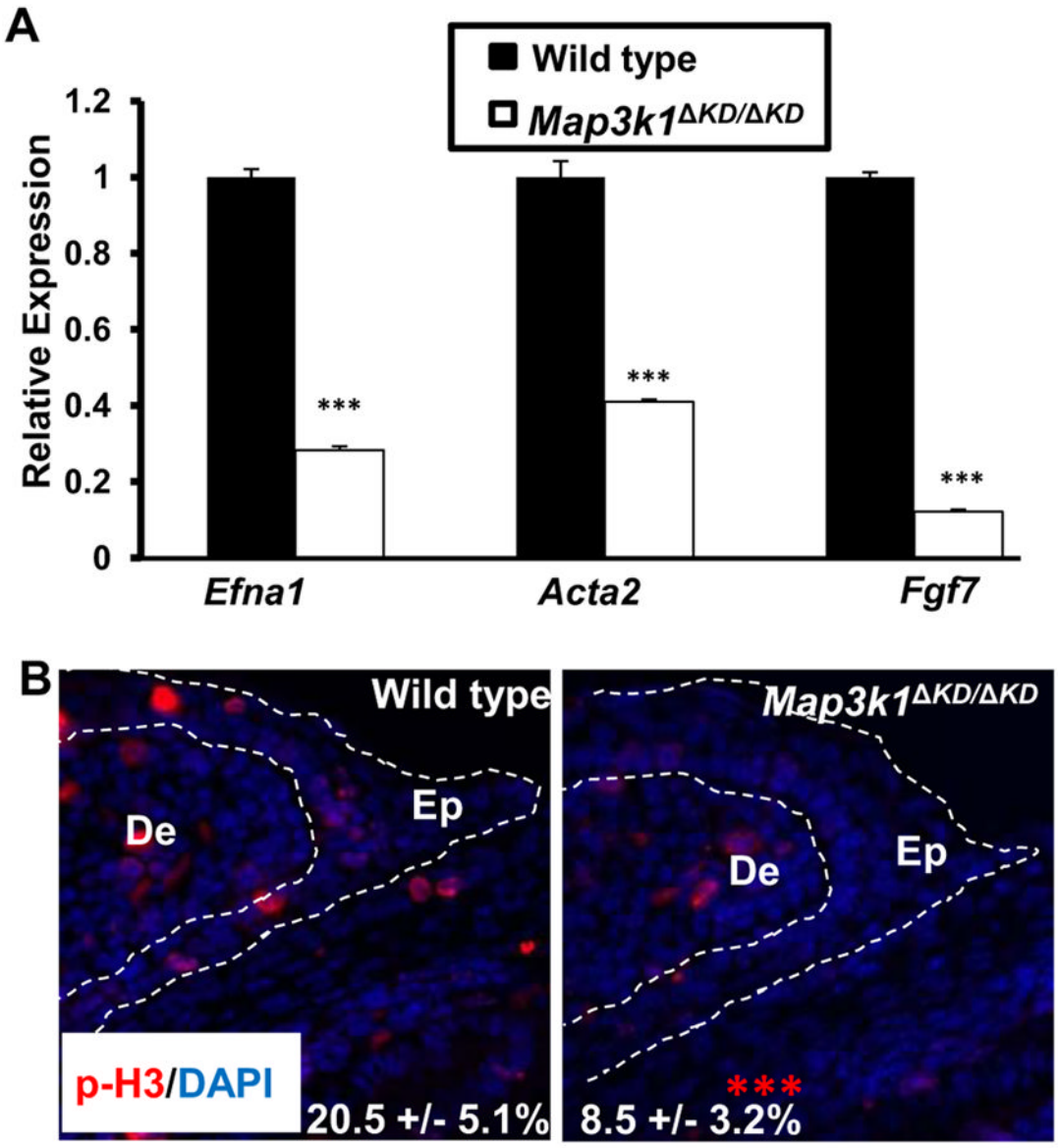

Figure 3. MAP3K1 regulates morphogenesis and H3 phosphorylation

(A) Wild type and *Map3k1*$^{\Delta KD/\Delta KD}$ fetuses at E15.5 were used for LCM and RNA isolation. Samples of LE eyelid epithelium were analyzed by qRT-PCR for specific genes as indicated. Results are shown as mean ± SD from at least 3 samples of each genotype and triplicate PCR of each sample. Relative expression was calculated as in Fig. 1. (B) The E15.5 wild type and *Map3k1*$^{\Delta KD/\Delta KD}$ fetuses were subjected to immunostaining using anti-phospho histone 3 (p-H3, Red) and nuclei were stained with Hoechst (Blue). Pictures were taken under Axio fluorescence microscopy. Dotted lines mark the eyelid epithelium (Ep) laying over the dermis (De). The percentage of pH3-positive cells in the tip of eyelid epithelium was calculated and the results are expressed as the mean ± SD from 6 wild type and 10 knockout eyes examined. Statistic analyses were done by Student *t-test,* ***$p < 0.001$ is considered significant.

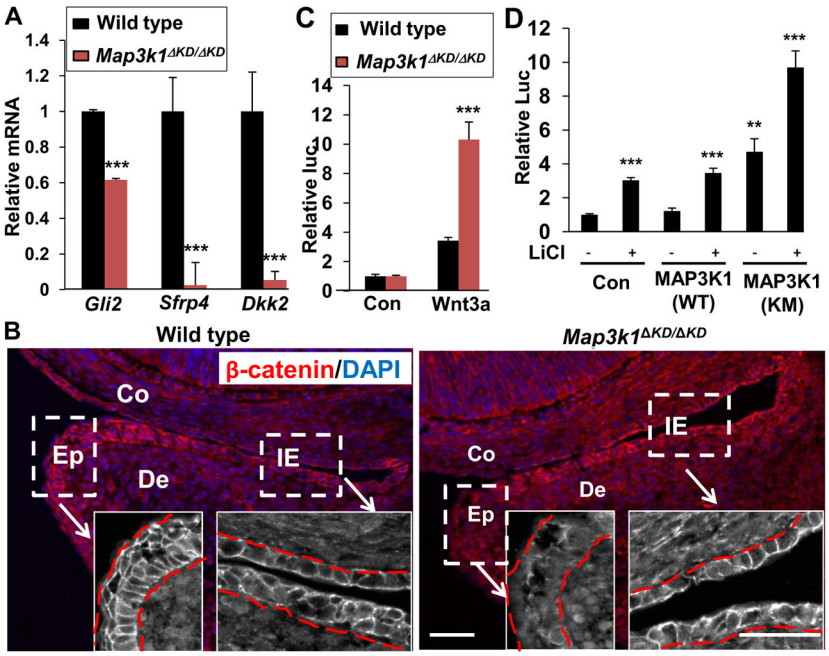

Figure 4. MAP3K1 regulates morphogenetic signaling pathways in LE eyelid epithelium

(A) Total RNA isolated from LE or IE epithelium of E15.5 wild type and *Map3k1*$^{\Delta KD/\Delta KD}$ fetuses were examined by qRT-PCR for mRNA of *Gli2* and *Sfrp4* in LE and *Dkk2* in IE cells. Relative expression was calculated as described in Fig. 1. The results shown are the mean ± SD from at least 3 samples of each genotype and triplicate PCR of each sample. Statistical analyses were done by Student *t-test,* ***p<0.001 was considered significant. (B) Wild type and *Map3k1*$^{\Delta KD/\Delta KD}$ fetuses at E15.5 were subjected to immunostaining using anti-β-catenin (Red) and nuclei were stained with Hoechst (Blue). Pictures were taken under low and high (insets) magnification. Dotted lines mark the boundary between epithelium and dermis. LE: leading edge eyelid; IE: Inner eyelid; De: Dermis; Co: cornea. Scale bar represents 50 μm. (C) Wild type and *Map3k1*$^{\Delta KD/\Delta KD}$fibroblasts were co-transfected with TCF/LEF-luc and CMV-renilla luciferase reporter plasmids in the presence or absence of plasmids for Wnt3a for 24 h, or (D) HEK293 cells were transfected with TCF/LEF-luc and CMV-renilla luciferase reporter plasmids in the presence or absence of expression vectors for MAP3K1(WT) or MAP3K1(KM) and of LiCl treatment for 24 h. The relative luciferase activity was calculated based on the ratio of firefly to renilla activities, with the values in control wild type cells or empty vector transfected untreated cells set as 1. Statistic analyses were done by Student *t-test,* ***p<0.001 are considered significant.

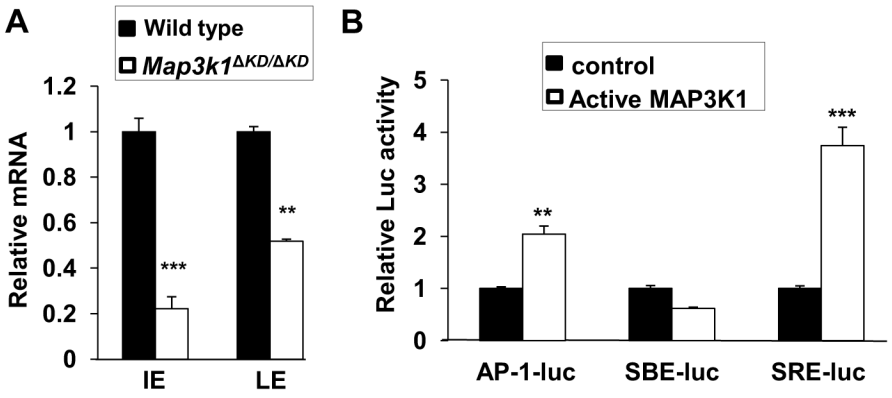

Figure 5. Transcription factors affected by MAP3K1

(A) Total RNA isolated from LE and IE epithelium of wild type and *Map3k1*$^{\Delta KD/\Delta KD}$ fetuses at E15.5 was used for qRT-PCR determination of *Ap2α* mRNA expression. relative to *Gapdh* and compared to the expression in wild type cells, set as 1. The results are shown as mean ± SD from at least 3 samples of each genotype and triplicate PCR of each sample. Statistical analyses were done by Student *t-test,* **p<0.01 and ***p<0.001 are considered significant. (B) HEK293 cells were transfected with luciferase reporter plasmids for the different transcription factors, together with a CMV-renilla luciferase reporter, with or without expression of active MAP3K1. The relative luciferase activity was calculated based on the ratio of firefly to renilla activities, with the values in control wild type cells set as 1. Statistical analyses were done by Student *t-test,* **p<0.01 and ***p<0.001 are considered significant. LE: leading edge eyelid; IE: Inner eyelid.

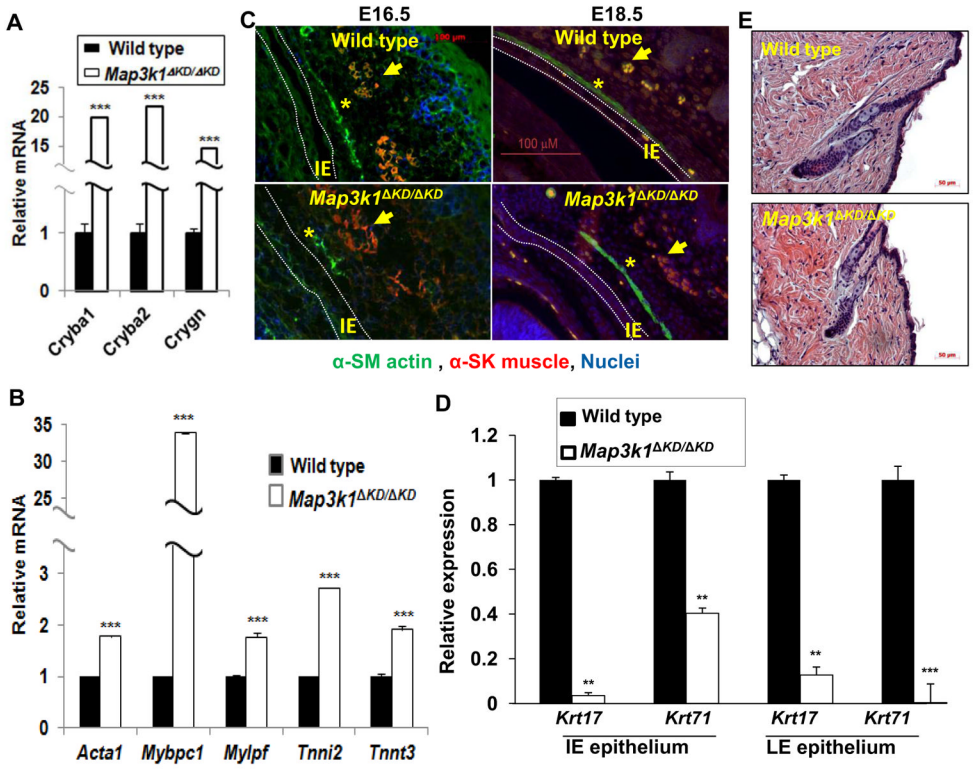

Figure 6. MAP3K1 affects differentiation of LE and IE eyelid epithelium

Total RNA isolated from (A) LE; (B) IE epithelium; and (D) both LE and IE cells of wild type and *Map3k1*$^{\Delta KD/\Delta KD}$ E15.5 fetuses were used for qRT-PCR using gene primers for (A) the lens crystallin genes indicated, (B) skeletal muscle genes, and (D) hair follicle genes. Relative expression was calculated as in Fig. 1. The results shown are the mean ± SD from at least 3 samples of each genotype and triplicate PCR of each sample. Statistical analyses were done by Student *t-test,* ***p<0.001 are considered significant. (C) The developing eyes of wild type and *Map3k1*$^{\Delta KD/\Delta KD}$ fetuses at E16.5 and E18.5 were examined by immunohistochemistry using anti-α2 actin (green) for smooth muscle (asterisks) and anti-SK myosin (red) for skeletal muscle (arrows). Nuclei were labeled with Hoechst (blue). Scale bar = 100μm. LE: leading edge eyelid; IE: Inner eyelid epithelium was marked with dotted lines. (E) Longitudinal haired skin sections of control and *Map3k1*$^{\Delta KD/\Delta KD}$ mice at P1. Epidermis, dermis, representative telogen hair follicles and adnexa display no overt structural abnormalities (H&E, Scale bar = 50μm).

Table I

Classification MAP3K1-regulated genes in LE and IE eyelid epithelium

MAP3K1-dependent genes in LE	
morphogenesis	GO:0048598, GO:0035239, GO:0010926, GO:0016331, GO:0048729, GO:0009888, GO:0048730, GO:0031069, GO:0060512, GO:0048858, GO:0007440, GO:0042733, GO:0060425, GO:0000902, GO:0010770, GO:0009790, GO:0001763, GO:0035239 GO:0060571, GO:0061138, GO:0042472, GO:0060572, GO:0042471, GO:0048646, GO:0045684, GO:0008544, GO:0045682, GO:0022612, GO:0002009, GO:0060443, GO:0048557, GO:0048596, GO:0048048, GO:0032989, GO:0003007, GO:0060740, GO:0009887, GO:0007435, GO:0060325, GO:0060562, GO:0060688, GO:0090103, GO:0010171, GO:0060323, GO:0048754,
proliferation	GO:0048146, GO:0002053, GO:0042127, GO:0010463, GO:0050679, GO:0010464, GO:0050678, GO:0048144, GO:2000179, GO:0008285, GO:0050673, GO:0021936, GO:0043616, GO:2000177, GO:0048145,
actin cytoskeleton	GO:0007010, GO:0030036, GO:0008092, GO:0005925, GO:0003779, GO:0015629, GO:0030029, GO:0032432, GO:0032970, GO:0030832, GO:0051017, GO:0030048, GO:0031532, GO:0001725, GO:0007010, GO:0007015, GO:0032956, GO:0008154, GO:0030042, GO:0030834, GO:0008064, GO:0051015,
hair follicle	GO:0001942, GO:0031069, GO:0022405, GO:0042633, GO:0042303
hedgehog pathway	GO:0007224, GO:0008589, GO:0045880
Wnt pathway	mmu04310, GO:0016055, GO:0060070, GO:0030178, GO:0060828, GO:0030111, GO:0090090, GO:0090263
Notch pathway	mmu04330
MAP3K1-repressed genes in LE	
lens	GO:0005212, GO:0002088
keratinocyte differentiation	GO:0001533, GO:0030216, GO:0030216, c2:1718
MAP3K1-dependent genes in IE	
morphogenesis	GO:0009887, GO:0048730, GO:0060425, GO:0060441, GO:0035239, GO:0003382, GO:0009887, GO:0048562, GO:0002009, c5:377, GO:0072088, GO:0048598, GO:0048729, GO:0048546, GO:0048704, GO:0060993, GO:0072028, GO:0035136, GO:0060571, GO:0032990, GO:0000904, GO:0048858, GO:0010927, GO:0048812, GO:0032989, GO:0000902, GO:0000904, c5:1089, GO:0048813, GO:0048814, GO:0010769, GO:0022604, GO:0048667,
intemediate filament	GO:0045104, c5:81, c5:290, c5:909, GO:0045103, GO:0032231, GO:0005882, GO:0045111, GO:0045109, GO:0045095, c5:89
Hair follicle	GO:0001942, GO:0031069, GO:0042633, GO:0022405
proliferation	GO:0008284, GO:0032944, GO:0050670, GO:0070663, GO:0042129, GO:0032943, GO:0046651, GO:0070661, GO:0042127, GO:0032946, GO:0050671
Wnt pathway	GO:0007223, mmu04310, GO:0030178
immunity	GO:0006955, GO:0002263, GO:0002366, c5:662, GO:0002697, c5:736, c2:117, c5:1113, c2:332, c2:262, c5:1615, mmu05320, GO:0002822, c5:495, c5:1199, GO:0002455, mmu04672, c5:854, GO:0002252, GO:0016064, GO:0002684, GO:0002699, GO:0002460, GO:0002250, GO:0006959, GO:0050776, GO:0002824, GO:0002821, GO:0002819, GO:0002682
proteinaceous extracellular matrix	GO:0005578, GO:0031012, GO:0044421, GO:0005615, c5:254
MAP3K1-repressed genes in IE	
striated muscle cell differentiation	GO:0051146, GO:0055002, mmu04260, GO:0060537, GO:0005865, c5:1063, c2:1227, GO:0003009, c5:46, c5:1040, GO:0051149, GO:0046716, c2:1154, c5:249, c2:212, GO:0006941, c2:1160
cytoskeleton organization	GO:0007010, GO:0030036, GO:0030029, GO:0003779, GO:0015629, c5:891, GO:0015630, c5:174, GO:0070507, c5:84, c5:354, GO:0051493, c2:1960, GO:0000226, mmu04810, c5:314, c2:242

Table II

MAP3K1-dependent genes in morphogenesis of LE eyelid epithelium

symbol	name	fold. wt vs ko	p. value
Morphogenesis			
Sfrp4	secreted frizzled-related protein 4	2.95	0.0246
Tdgf1	teratocarcinoma-derived growth factor 1	2.21	0.00231
Krt17	keratin 17	2.18	0.00178
Krt27	keratin 27	2.13	0.0364
Dmp1	dentin matrix protein 1	2.06	0.0367
Arhgdia	Rho GDP dissociation inhibitor (GDI) alpha	2	0.0371
Mapk14	mitogen-activated protein kinase 14	1.79	0.0224
Fgf7	fibroblast growth factor 7	1.7	0.00466
Gli2	GLI-Kruppel family member GLI2	1.68	0.00222
Efna1	ephrin A1	1.67	0.0443
Spry2	sprouty homolog 2 (Drosophila)	1.64	0.00334
Trps1	trichorhinophalangeal syndrome I (human)	1.61	0.00281
Inpp5k	inositol polyphosphate 5-phosphatase K	1.58	0.0157
Gnaq	guanine nucleotide binding protein, aq polypeptide	1.57	0.0129
Cbfa2t2	core-binding factor, runt domain, a2	1.52	0.0161
Aqp1	aquaporin 1	1.5	0.00721
Fgf9	fibroblast growth factor 9	1.5	0.0277
Hoxd8	homeo box D8	−1.57	0.006
Gamt	guanidinoacetate methyltransferase	−1.62	0.00609
Lor	loricrin	−1.62	0.0063
Ift52	intraflagellar transport 52 homolog	−1.65	0.0269
Ednrb	endothelin receptor type B	−1.72	0.0343
Tgfbr1	transforming growth factor, beta receptor I	−1.75	0.0442
Chl1	cell adhesion molecule homology to L1CAM	−1.76	0.00862
Nr3c1	nuclear receptor subfamily 3, group C, member 1	−1.85	0.00392
Hes1	hairy and enhancer of split 1 (Drosophila)	−1.86	0.0119
Ermn	ermin, ERM-like protein	−2.07	0.0214
Serpina1b	serine preptidase inhibitor, clade A, member 1B	−2.12	0.0246
Crygs	crystallin, gamma S	−2.16	0.012
Aldh1a1	aldehyde dehydrogenase family 1, subfamily A1	−2.65	0.000419
Cryaa	crystallin, alpha A	−2.92	0.0184
Ntf3	neurotrophin 3	−2.96	0.0184
Vpreb1	pre-B lymphocyte gene 1	−7.5	0.00505
Actin cytoskeleton			
Krt17	keratin 17	2.18	0.00178
Acta2	actin, alpha 2, smooth muscle, aorta	2.06	0.00798
Palld	palladin, cytoskeletal associated protein	1.77	0.0171
Gmfb	glia maturation factor, beta	1.73	0.00259

symbol	name	fold. wt vs ko	p. value
Fgf7	fibroblast growth factor 7	1.7	0.00466
Aqp1	aquaporin 1	1.5	0.00721
Fgd4	FYVE, RhoGEF and PH domain containing 4	−1.53	0.0253
Cryab	crystallin, alpha B	−1.71	0.00509
6330503K22Rik	RIKEN cDNA 6330503K22 gene	−2	0.00393
Ermn	ermin, ERM-like protein	−2.07	0.0214
Tnnt3	troponin T3, skeletal, fast	−2.25	0.0169
Cryaa	crystallin, alpha A	−2.92	0.0184
Tac1	tachykinin 1	−3	0.00299
S100a9	S100 calcium binding protein A9 (calgranulin B)	−3.71	0.0274

Table III

The morphogenetic pathways affected by MAP3K1

symbol	name	fold	p. value
LE		**wt vs ko**	
Wnt pathway			
Sfrp4	secreted frizzled-related protein 4	2.95	0.0246
1500003O03Rik	RIKEN cDNA 1500003O03 gene	1.87	0.0322
Nkd1	naked cuticle 1 homolog (Drosophila)	1.58	0.0161
Ddb1	damage specific DNA binding protein 1	1.5	0.0436
Fgf9	fibroblast growth factor 9	1.5	0.0277
Rnf138	ring finger protein 138	1.53	0.0205
Rbx1	ring-box 1	1.64	0.0144
Shh pathway			
Gli2	GLI-Kruppel family member GLI2	1.68	0.00222
Fgf9	fibroblast growth factor 9	1.5	0.0277
Ift52	intraflagellar transport 52 homolog	1.65	0.0269
IE			
Wnt pathway			
Dkk2	dickkopf homolog 2 (Xenopus laevis)	1.69	0.0075

Table IV

SRF and AP-2 expression in LE cells

symbol	name	fold. wt vs ko	p. value
SRF in LE			
Srf	serum response factor	−1.04	0.7823
Srfbp1	serum response factor binding protein 1	−1.39	0.0704
SRF partners in LE			
Tfpt	TCF3 (E2A) fusion partner	1.509	0.0967
Tcf12	transcription factor 12	1.363	0.0385
Tcf15	transcription factor 15	1.032	0.7785
Tcf19	transcription factor 19	1.128	0.422
Tcf20	transcription factor 20	1.13	0.3011
Tcf21	transcription factor 21	−1.3	0.4408
Tcf23	transcription factor 23	−1.05	0.6353
Tcf25	transcription factor 25	1.169	0.1573
Tcf3	transcription factor 3	1.258	0.1188
Tcf4	transcription factor 4	1.195	0.2864
Tcf7	transcription factor 7, T-cell specific	−1.03	0.8015
Tcf7l2	transcription factor 7-like 2,	1.734	0.0735
AP-2 in LE			
Tcfap2a	transcription factor AP-2, alpha	1.178	0.3622
Tcfap2b	transcription factor AP-2 beta	1.351	0.0509
Tcfap2c	transcription factor AP-2, gamma	−1.06	0.6286
Tcfap2d	transcription factor AP-2, delta	−1.06	0.7004
Tcfap2e	transcription factor AP-2, epsilon	−1.01	0.9652
AP-2 in IE			
Tcfap2a	transcription factor AP-2, alpha	1.692	0.0034
Tcfap2b	transcription factor AP-2 beta	1.484	0.0098
Tcfap2c	transcription factor AP-2, gamma	1.124	0.2165
Tcfap2d	transcription factor AP-2, delta	−1.9	0.4026
Tcfap2e	transcription factor AP-2, epsilon	1.016	0.2511

Table V

Differentiation programs affected by MAP3K1

symbol	name	fold wt vs ko	p. value
LE epithelium			
Hair follicle			
Krt17	keratin 17	2.18	0.00178
Krt27	keratin 27	2.13	0.0364
Fgf7	fibroblast growth factor 7	1.7	0.00466
Lens crystallin			
Cryaa	crystallin, alpha A	−2.92	0.0184
Cryab	crystallin, alpha B	−1.71	0.00509
Cryba1	crystallin, beta A1	−3.35	0.00645
Cryba2	crystallin, beta A2	−4.71	0.0188
Crybb1	crystallin, beta B1	−1.95	0.0392
Cryge	crystallin, gamma E	−2.83	0.00108
Crygf	crystallin, gamma F	−1.81	0.00983
Crygn	crystallin, gamma N	−3.69	0.0336
Crygs	crystallin, gamma S	−2.16	0.012
Lim2	lens intrinsic membrane protein 2	−1.62	0.00414
IE epithelium			
Hair follicle			
Krt71	keratin 71	2.17	0.0106
Krt25	keratin 25	1.96	0.00253
Krt27	keratin 27	1.9	0.00839
Tchh	trichohyalin	2.16	0.00466
Krtap7-1	keratin associated protein 7-1	1.93	0.0258
Krt73	keratin 73	1.67	0.0156
Muscle differentiation			
Murc	muscle-related coiled-coil protein	−1.52	0.0102
Rb1	retinoblastoma 1	−1.57	0.00341
Mef2c	myocyte enhancer factor 2C	−1.61	0.00766
Zfp238	zinc finger protein 238	−1.71	0.00389
Atp1b4	ATPase, (Na+)/K+ transporting, b 4	−1.84	0.0168
Acta1	actin, alpha 1, skeletal muscle	−2.27	0.0474
Mylpf	myosin light chain fast skeletal	−2.51	0.0458
Mybpc1	myosin binding protein C	−2.63	0.0392
Tnni2	troponin I, skeletal, fast 2	−2.74	0.0316
Tnnt3	troponin T3, skeletal, fast	−3.76	0.0162

Table VI

MAP3K1-dependent genes enriched for SRF binding sites

symbol	name	fold. wt vs ko	p. value
Krt17	keratin 17	2.18	0.00178
Acta2	actin, alpha 2, smooth muscle, aorta	2.06	0.00798
Pcdhb15	protocadherin beta 15	1.98	0.0221
Olfr1290	olfactory receptor 1290	1.89	0.0172
Tagln	transgelin	1.84	0.0159
Ndufa7	NADH dehydrogenase (ubiquinone) 1a7	1.83	0.035
Mapk14	mitogen-activated protein kinase 14	1.79	0.0224
Dcaf8	DDB1 and CUL4 associated factor 8	1.73	0.0162
Fgf7	fibroblast growth factor 7	1.7	0.00466
U2af1l4	U2 small nuclear RNA auxiliary factor 1– 4	1.67	0.0467
Sertad4	SERTA domain containing 4	1.64	0.0088

Table VII

MAP3K1 regulates differentiation programs *in vitro*.

symbol	name	fold wt vs ko	p. value
Mylpf	myosin light chain, fast skeletal muscle	−4.8277	0.0002
Myh3	myosin, heavy polypeptide 3, skeletal muscle	−3.0509	0.0013
Acta1	Actin, alpha 1, skeletal muscle	−2.6842	0.0161
Spna1	spectrin alpha 1	−2.2766	0.0002
Gys1	glycogen synthase 1, muscle	−2.2114	0.0003
Tnnt1	troponin T1, skeletal, slow	−1.512	0.0009
Pygm	muscle glycogen phosphorylase	−1.5113	0.0003
Eno3	Enolase 3, beta muscle	−1.4896	0.0028
Tnnc2	troponin C2, fast	−1.4392	0.0235